

F-9-3

Pentacene TFTs Fabricated by High-aspect Ratio Metal Shadow Mask

Sung Hun Jin, Sang Min Yi*, Keum Dong Jung, Chang Bum Park, Chong Nam Chu*, Hyung Chul Shin, Byung-Gook Park, and Jong Duk Lee

Inter-university Semiconductor Research Center and School of Electrical Engineering, Seoul National University,
School of Mechanical and Aerospace Engineering, Seoul National University*,
San 56-1, Shinlim-dong, Kwanak-gu, Seoul 151-742, Korea

Phone: +82-2-880-7282 Fax: +82-2-882-4658 E-mail: harin74@dreamwiz.com

1. Introduction

Among various organic semiconductors, pentacene continues to be an attractive material choice because of its high mobility on the order of $1 \text{ cm}^2/\text{Vsec}$ for a variety of electronic applications, including information displays [1-3], electronic paper [4], and radio frequency identification (RFID) [5]. Even though pentacene thin film transistors (TFTs) can be implemented in one of two configurations, i.e., top contact and bottom contact [6], the best performances of pentacene TFTs in the literature [7,8] have always been demonstrated in the top contact configuration due to the inherently favorable conditions of pentacene growth compared with bottom contact mode [6]. However, the top contact mode is incompatible with the conventional photolithography for the definition of source and drain (S/D) electrodes on organic semiconductors due to their intolerance to the exposure of solvents and other liquids [9]. Therefore, metal shadow masks are generally used to define the top S/D contacts on organic materials because they can guarantee simple S/D definition process without damage of organic materials. But the S/D patterning process by the conventional metal shadow mask ($L_C \approx 20\text{--}70 \text{ }\mu\text{m}$) [6], [9] has two major obstacles, which are high-resolution patterning [10] and mass manufacturability. While commercial products like OLED eliminate gradually the pessimistic prospect for the applications of a metal shadow mask to mass production [11], the high-resolution patterning using shadow masks can be a remaining barrier on highly integrated top-contact OTFTs [8].

To achieve top-contact OTFTs with a high areal density, several approaches including cold welding [12], high resolution rubber stamping [13] and special Si membrane masks ($L_C \approx 10 \text{ }\mu\text{m}$) [14] have been reported in the literature, whereas each method has fundamental drawbacks of too much-complicated implementation [12], low-level manufacturability for large area applications [13], and easy brittleness [14].

In this work, we proposed and implemented metal shadow masks with a high aspect ratio (AR) larger than 20, based on a combination of anisotropic micro-electro-discharge machining ($\mu\text{-EDM}$) [15] and isotropic electro chemical etching (ECE) [16] for the application of OTFTs scaled down to less than $5 \text{ }\mu\text{m}$. The high-aspect ratio (HR) metal shadow masks have inherent merits of structural robustness, simple S/D patterning process, and re-usage. In addition, a batch mode $\mu\text{-EDM}$ technique [17] can be fundamentally applicable to metals shadow masks of a high throughput and good uniformity for large area applications.

2. Experimental and Results

Figure 1 presents a schematic illustration of (a) $\mu\text{-EDM}$ [15] and (b) ECE [16], which were used to fabricate metal shadow masks with high AR larger than 20. As shown in Fig. 1(a), an AR for a metal shadow mask is defined as the thickness of a shadow mask (T_S) to the length of a bridge (L_C). In this experiment, $\mu\text{-EDM}$ system used the applied voltage of 100 V, a single RC pulse timing circuits with 500 pF and 1 k Ω , and a square copper electrode with one side length of $130 \text{ }\mu\text{m}$ and structural height of $1500 \text{ }\mu\text{m}$ fabricated by wire electrode discharge gliding (WEDG)[18]. The work pieces for shadow masks are $100 \pm 5 \text{ }\mu\text{m}$ thick stainless steel (304 SS) with the size of $1.5 \text{ cm} \times 1.5 \text{ cm}$. After serially machining

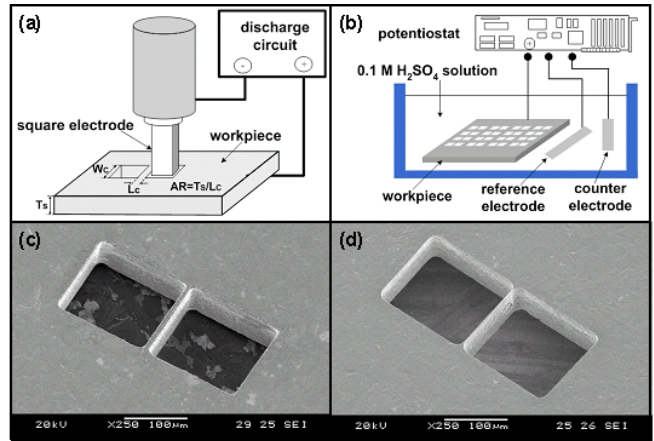


FIG 1. Schematic configurations for (a) micro-electro-discharge machining ($\mu\text{-EDM}$) and (b) electro-chemical etching (ECE). The aspect ratio (AR) of an HR shadow mask denotes the ratio of the thickness of workpiece (T_S) to the length of a bridge (L_C). After $\mu\text{-EDM}$ processing up to the channel length of $10 \text{ }\mu\text{m}$, the work piece consecutively was electro chemically etched with an etch rate of $4.4 \text{ }\text{\AA}/\text{sec}$ in $0.1 \text{ mole H}_2\text{SO}_4$ solution (c) A SEM image for a stainless steel shadow mask right after $\mu\text{-EDM}$ process. After $\mu\text{-EDM}$ process, L_C is $10 \text{ }\mu\text{m}$ with an aspect ratio of 10 (d) A SEM image for a metal shadow mask right after $\mu\text{-EDM}$ and ECE process. L_C is $3.5 \text{ }\mu\text{m}$ with an aspect ratio of 28. The width of bridge (W_C) is $150 \text{ }\mu\text{m}$.

$150 \text{ }\mu\text{m}$ square contact holes using $\mu\text{-EDM}$, the combinational process of ECE improves the AR of a metal shadow mask noticeably because the $\mu\text{-EDM}$ has a fundamental limit of the routinely machinable feature size ($L_C \approx 10 \text{ }\mu\text{m}$) as shown in Fig. 1(c). Figure 1(b) shows that process conditions of ECE system are the applied voltage of 1.2 V and the $0.1 \text{ mole H}_2\text{SO}_4$ solution as electrolyte. Figure 1 (c) and (d) showed SEM images for a metal shadow mask after $\mu\text{-EDM}$ and ECE steps, respectively. To date, the length (L_C) and width (W_C) of the bridge can be routinely obtained as small as $5 \pm 0.25 \text{ }\mu\text{m}$ and $70 \pm 1 \text{ }\mu\text{m}$, respectively.

Figure 2(a) shows a schematic for the fabrication steps of pentacene TFTs. For a gate insulator, 35 nm thick thermal oxide was grown on a p-type wafer with the resistivity of $15 \text{ }\Omega\text{cm}$. The thermal oxide was patterned by photolithography, and then etched by dilute HF solution for a gate electrode deposition. After cutting the patterned Si wafer to the size of $2 \text{ cm} \times 2 \text{ cm}$, each sample was spin-coated with a dilute PMMA solution to improve the ordering of pentacene due to the hydrophobic ending group methyl radical ($-\text{CH}_3$) [19]. The coated PMMA thickness was 10 nm as measured by ellipsometry. A 50 nm thick pentacene was thermally evaporated on the PMMA treated gate oxide at a rate of about $0.3 \text{ }\text{\AA}/\text{sec}$. During the deposition, the substrate temperature maintained at the temperature of $90 \text{ }^\circ\text{C}$ in the pressure of $8 \times 10^{-8} \text{ torr}$. The pentacene of about $98 \text{ }\%$ purity was used without purification in this experiment. Finally 50 nm of gold was e-beam evaporated on pentacene active layer through a $100 \text{ }\mu\text{m}$ thick HR shadow mask to define S/D contacts as well as the gate contacts. The dimension of source and drain contacts have the channel length ranging from $20 \text{ }\mu\text{m}$ to $5 \text{ }\mu\text{m}$ at a fixed channel width of $150 \text{ }\mu\text{m}$.

Figure 2 (b) shows the AFM image of channel area for an OTFT with $W_C = 150 \text{ }\mu\text{m}$ and $L_C = 5 \text{ }\mu\text{m}$. As shown in Fig. 2 (b), the

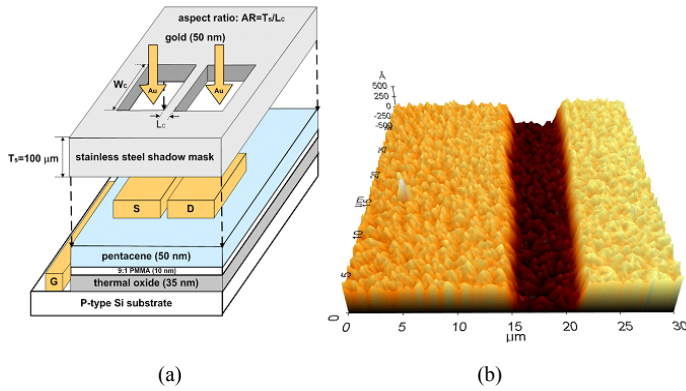


FIG 2. (a) Schematic illustration of process steps for pentacene TFTs fabricated using an HR metal shadow mask. The length of a bridge (L_C) for metal shadow masks ranges from 20 μm to 5 μm with a fixed channel width of 150 μm (b) An AFM image for the defined channel area of OTFT with $L_C=5 \mu\text{m}$ and $W=150 \mu\text{m}$.

defined source and drain contacts have a good straight channel.

Figure 3 (a) shows the transfer characteristics of OTFTs with a different L_C of 5 and 20 μm for a fixed W_C of 150 μm in the saturation region. For the device with L_C of 20 μm , electrical parameters are the threshold voltage (V_{TH}) of -1.3 V, subthreshold swing (SS) of 1.2 V/decade, current on-off ratio of 7.1×10^6 , field effect mobility (μ_{eff}) of $0.421 \pm 0.07 \text{ cm}^2/\text{Vsec}$ at gate-source voltage (V_{GS}) of -10 V and drain-source voltage (V_{DS}) of -20 V. On the other hand, the device with L_C of 5 μm has V_{TH} of 3.3 V, SS of 1.2 V/decade, μ_{eff} of $0.498 \pm 0.05 \text{ cm}^2/\text{Vsec}$ at the same V_{GS} and V_{DS} . As the L_C of OTFT reduces from 20 μm to 5 μm , V_{TH} was shifted toward positive voltage from -1.3 V to 3.3 V. The current on-off ratio and SS was deteriorated from 7.1×10^6 to 1.6×10^5 and from 1.2 V/decade to 5.7 V/decade, respectively.

The result is thought to be attributed to the scaling-down effects of OTFTs, i.e. short channel effect [20], which V_{TH} increases from negative voltage to positive voltage as L_C decreases. In addition, the hump effects [21] of OTFTs fabricated by the HR shadow mask having $L_C=5 \mu\text{m}$ enhance the conspicuous change of V_{TH} , SS and current on-off ratio because the parasitic OTFT with $L_C=2.5 \mu\text{m}$ is turned on before the main OTFT with $L_C=5 \mu\text{m}$ as shown in Fig. 3 (b). Figure 3(b) shows that the L_C has locally abnormal channel of 2.5 μm in the OTFT due to the strong electric field around the corner of electrode during μ -EDM process.

Figure 4 shows the output characteristics of pentacene TFTs with L_C of (a) 5 μm and (b) 20 μm . For the OTFTs with $L_C=5 \mu\text{m}$ and $L_C=20 \mu\text{m}$ at $V_{GS}=-10 \text{ V}$ and $V_{DS}=-20 \text{ V}$, the saturated drain current (I_{DSS}) was $I_{DSS}=-24 \mu\text{A}$ and $I_{DSS}=-4 \mu\text{A}$, respectively. The measured saturation current ratio of $(-24 \mu\text{A})/(-4 \mu\text{A})$ was obtained as 6. The significant improvement of current drivability was achieved from scaling down L_C from 20 μm to 5 μm at the same W_C of 150 μm . The result is meaningful because OTFTs of high current drivability consuming the same layout-area are highly demanded to achieve high-resolution flat panel displays based on OTFTs.

3. Conclusions

Metal shadow masks with a high aspect ratio ($AR>20$) using micro-EDM and ECE were proposed for high definition of S/D contacts ($L \leq 5 \mu\text{m}$ and $W \leq 150 \mu\text{m}$) on organic semiconductors. The fabricated pentacene TFTs with the channel length of about 5 μm showed routinely mobility of $0.49 \pm 0.025 \text{ cm}^2/\text{Vsec}$ and current on-off ratio of 10^5 . The HR metal shadow masks with AR larger than 20 can be used repeatedly for S/D electrodes deposition due to the structural robustness. The pentacene TFTs by HR shadow masks can meet the required OLED pixel resolution ($\leq 100 \times 100 \mu\text{m}^2$) as well as high current drivability through the scaling-down of the width of OTFTs [11]. In addition, a batch mode μ -EDM can

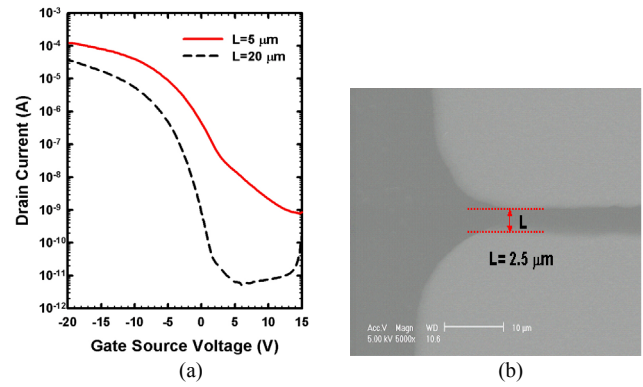


FIG 3. (a) Transfer characteristics of pentacene TFTs with $L_C=5 \mu\text{m}$ and $L_C=20 \mu\text{m}$ in the saturation region (b) a SEM image for the locally abnormal parasitic OTFT with $L_C=2.5 \mu\text{m}$.

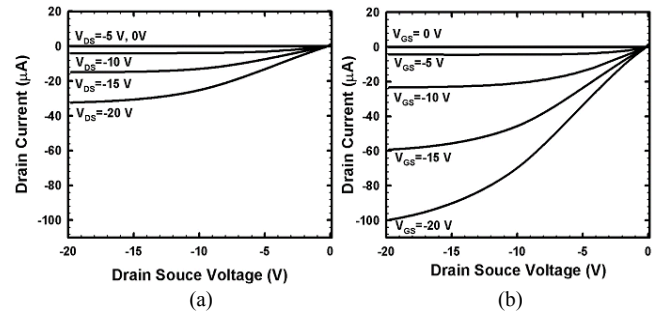


Fig. 4. Output characteristics of pentacene TFTs with (a) $L_C=20 \mu\text{m}$ and (b) $L_C=5 \mu\text{m}$ for a fixed channel width of 150 μm .

potentially solve a throughput and yield problem of HR metal shadow mask generation.

Acknowledgements

This work was supported by the contract of ISRC (Inter-University Semiconductor Research-Center) 2002-X-5505 to ETRI (Electronics and Telecommunications Research Institute) and MIC (Ministry of Information and Communication) to carry out the Advanced Technology Project.

References

- [1] P. Mach, et al., *Appl. Phys. Lett.*, vol. 78, pp. 3592, 2001.
- [2] C. D. Sheraw, et al., *Appl. Phys. Lett.*, vol. 80, pp. 1088, 2002.
- [3] E. A. Huiteman, et al., *Adv. Mater.*, vol. 14, pp. 1201, 2002.
- [4] Gerwin H. Gelinck, et al., *Nature Mat.*, vol. 3, pp. 106, 2004.
- [5] P. F. Baude, et al., *Appl. Phys. Lett.*, vol. 82, pp. 3964, 2003.
- [6] Ioannis Kyriassis, et al., *IEEE Trans. Electron Devices*, vol. 48, pp. 1060, 2001.
- [7] Hagen Klauk, et al., *J. Appl. Phys.*, vol. 9, pp. 5259, 2002.
- [8] Paul F. Baude, et al., *IEDM Techn. Dig.*, 8. 1, 2003.
- [9] D. J. Gundlach, et al., *Appl. Phys. Lett.*, vol. 74, pp. 3302, 1999.
- [10] G. J. Burger, et al., *Sensors and Actuators*, A 54, pp. 669, 1996.
- [11] E. Becker, et al., *Appl. Phys. Lett.*, vol. 82, pp. 2712, 2003.
- [12] Changsoon Kim, et al., *Appl. Phys. Lett.*, vol. 80, pp. 4051, 2002.
- [13] Jana Zaumseil, et al., *Appl. Phys. Lett.*, vol. 82, pp. 793, 2003.
- [14] C. D. Dimitrakopoulos, et al., *Science*, vol. 283, pp. 822, 1999.
- [15] T. Masaki, K. Kawata, et al., *Proc. IEEE Int. Workshop on Micro Electro Mechanical Systems (MEMS'90)*, pp. 21, 1990.
- [16] M. Datta, et al., *IBM J. Res. Develop.*, vol. 42, pp. 655, 1998.
- [17] Ken'ichi Takahata, et al., *J. MEMS*, vol. 11, pp. 102, 2002.
- [18] Masuzawa, et al., *Annals of the CIRP*, vol. 34, pp. 431, 1985.
- [19] Sung Hun Jin, et al., *J. Kore. Phy. Soc.*, vol. 44, pp. 185, 2004.
- [20] L. Torsi, et al., *J. Appl. Phys.*, vol. 78, pp. 1088, 1995.
- [21] P. Sallagoity, et al., *IEEE Trans. Electron Devices*, vol. 43, pp. 1900, 1996.
- [22] Christos D. Dimitrakopoulos, et al., *Adv. Mater.*, vol. 14, pp. 99, 2002.